



HAL
open science

Silicon based photo-controlled deformable mirror

Lorenzo Cabona, Edoardo Redaelli, Frederic Zamkotsian, Giorgio Pariani,
Patrick Lanzoni, Andrea Bianco

► **To cite this version:**

Lorenzo Cabona, Edoardo Redaelli, Frederic Zamkotsian, Giorgio Pariani, Patrick Lanzoni, et al.. Silicon based photo-controlled deformable mirror. *Optics and Lasers in Engineering*, 2022, 153, pp.106993. 10.1016/j.optlaseng.2022.106993 . hal-04310694

HAL Id: hal-04310694

<https://hal.science/hal-04310694>

Submitted on 28 Nov 2023

HAL is a multi-disciplinary open access archive for the deposit and dissemination of scientific research documents, whether they are published or not. The documents may come from teaching and research institutions in France or abroad, or from public or private research centers.

L'archive ouverte pluridisciplinaire **HAL**, est destinée au dépôt et à la diffusion de documents scientifiques de niveau recherche, publiés ou non, émanant des établissements d'enseignement et de recherche français ou étrangers, des laboratoires publics ou privés.

Silicon based photo-controlled deformable mirror

Lorenzo Cabona¹, Edoardo Redaelli¹, Frederic Zamkotsian², Giorgio Pariani¹, Patrick Lanzoni², Andrea Bianco¹

¹INAF – Osservatorio Astronomico di Brera, Via Bianchi 46, 23807 Merate, Italy

²Aix Marseille Université, CNRS, CNES, LAM (Laboratoire d'Astrophysique de Marseille), 13388, Marseille, France

Abstract

The fabrication and characterization of a Silicon based photo-controlled deformable mirror (PCDM) for spatial light modulation and wavefront control is reported. The device is a membrane mirror based on a 1-inch monolithic non-pixelated Silicon photoconductive substrate with a transparent ITO electrode on one side coupled with a 5 μm thick nitrocellulose membrane. The device is driven applying an AC voltage and it is characterized by measuring the generated wavefront using a Shack-Hartmann wavefront sensor. Upon uniform illumination with a NIR LED, the deformation increases with the voltage applied, its frequency and the light intensity. The maximum deformation achieved is approximately 2 μm PtV (wavefront). The repeatability of the induced deformation is also evaluated together with its time stability, proving that the device is reliable in the working conditions. The response time is evaluated and it is in the range of 10 ms. The device is suitable for an efficient adaptable focusing element with an important focus control.

Keyword: Deformable mirror, Photo-controlled deformable mirror, Wavefront shaping, Adaptive Optics.

1. Introduction

Deformable mirrors are optical devices that are finding an increasing interest in a wide range of applications including wavefront correction [1], temporal and spatial beam-shaping [2], and active and adaptive optics [3]. In the case of astronomical telescopes, they allow for correcting aberrated wavefronts (by the atmosphere or the inhomogeneous medium) and reach a better resolution of the optical system [4]. This is especially true for large size telescopes that have a very high theoretical resolution. This is possible thanks to the capability of such devices to modify their optical surface by suitable actuating systems [5]. Conventional technologies for the decimetres DMs are mainly based on two actuation processes: electromagnetic for the telescope adaptive secondary mirrors, piezoelectric for the DMs in the AO modules; the first ones are built around voice coils and thin shell mirrors [5] [6], the second ones use stack actuators [7], or annular PZT (Lead Zirconate Titanate) layers for unimorph bimorph DMs [8]. The development of new technologies based on micro-opto-electro-mechanical systems (MOEMS) is promising for future centimetre-size DMs. Their major advantages are compactness, scalability, and specific task customization using

elementary building blocks [9]. The MOEMS technology permits the development of a complete generation of new mirrors. Four main Micro-Deformable Mirrors (MDM) architectures are under study in different laboratories and companies, and they are based on single-crystalline and poly-crystalline silicon materials for defining the structural layers, i.e. mirrors, restoring beams, and hinges.

First, the bulk micro-machined continuous-membrane deformable mirror, studied by Delft University and OKO company, is a combination of bulk silicon micromachining with standard electronics technology [10]. This mirror is composed by a thin flexible conducting membrane, coated with a reflective material, and stretched over an electrostatic electrode structure. This mirror shows a very good mirror quality, but the mean deformed surface is concave, and the number of actuators cannot be scaled up to hundreds. Second, the segmented, micro-electro-mechanical deformable mirror manufactured by Iris AO [11] consists of a set of segmented piston-tip-tilt moving surfaces, fabricated in a dense array. Third, the surface micro-machined continuous-membrane deformable mirror made by Boston Micromachines Corporation (BMC) is based on a single compliant optical membrane supported by multiple attachments to an underlying array of surface-normal electrostatic actuators [12]. The efficiency of this device has been demonstrated recently in several AO system for astronomy, including the GPI instrument on Gemini telescope [13]. The third concept is certainly the most promising architecture, but it shows limited strokes for large driving voltages, and mirror surface quality may need further improvement for Extreme AO. Another interesting technology is the one employed in the ALPAO DMs [14], that are based on continuous reflective surface deformed by magnetic actuators, in this case the maximum stroke for tip/tilt reaches $\pm 90 \mu\text{m}$.

In all the above-mentioned technologies the density of actuators cannot be increased independently of the technology. Besides these technologies a deformable mirror can be realized using a large and continuous metalized membrane and a monolithic nonpixelated photoconductive substrate with the possibility to avoid the presence of real, physical actuators. Such devices are called Photo Controlled Deformable Mirrors (PCDMs).

The PCDM is an electrostatic deformable mirror, composed by a thin reflective membrane suspended above and electrically coupled to a photoconductive slab [15] [16]. When the photoconductive slab is illuminated with a light pattern, a change in the electrostatic pressure is produced in the illuminated areas of the photoconductor, which locally modifies the shape of the membrane (see Figure 1). Appropriately managing the light pattern illuminating the photoconductor, it is possible to define the size, shape and density of actuators, without the spatial segmentation into discrete elements inevitably present using the other deformable mirrors technologies [15].

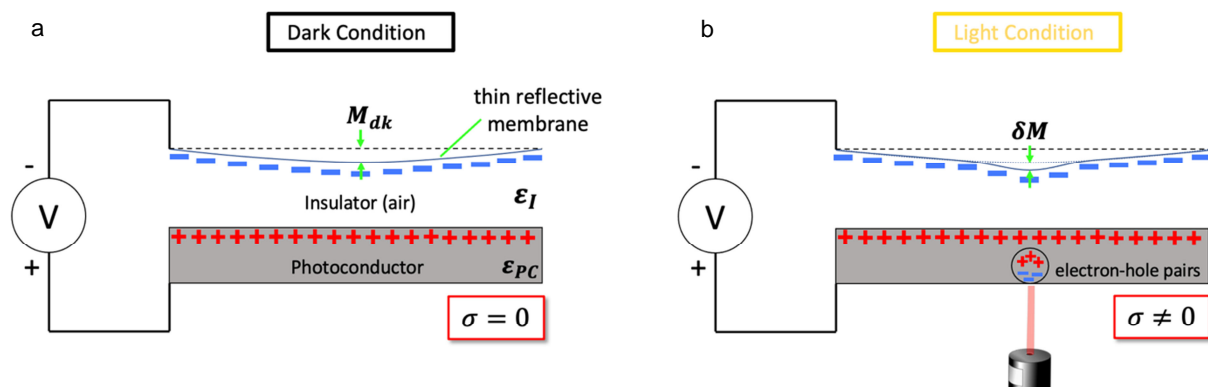


Figure 1: scheme of the functioning of a PCDM. (a) The deformation of the membrane due to the applied tension in dark condition; (b) deformation of the membrane when the photoconductor is illuminated by the light beam, in this last situation the deformation due to the photogenerated electron-hole pairs is superimposed on the previous deformation.

The particular design of the PCDM takes advantage of well-developed light projection techniques, allowing to decouple the driving electronics from the mirror actuation. This may be a huge advantage in comparison to usual AO mirrors that have a bulky and complex electronics. This turns into a potential reduction of cost, weight and space occupied by mechanical actuators [17]. These features make the PCDM technology very attractive in those situations where the weight and volume of the deformable mirror must be reduced [18] [19].

PCDMs have been manufactured using crystalline inorganic photoconductors such as Gallium Arsenide (GaAs), Indium phosphide (InP) [20], Bismuth-Silicon-Oxyde (BSO) [17][15], Zinc Selenide (ZnSe) [21] and, more recently, using an organic photoconductor consisting in a mixture of P3HT/PCBM doped with an arylamine (m-MTDATA) dispersed in a polystyrene matrix [22]. A model which identifies the key parameters that affect their performances is reported in the literature [15]. To the best of our knowledge, silicon has not been used so far for building a PCDM. This material is attractive for the high charge mobility; moreover, it is easy to find at a relatively low price and in large formats.

In this paper, we show the manufacturing of a 1-inch silicon based PCDM and its characterization in terms of deformation as function of the driving parameters. In addition, the response time is evaluated.

2. Material and methods

2.1 Photoconductor

The photoconductor is a round 1-inch undoped silicon substrate manufactured by UniversityWafer, Inc. The main properties of the photoconductor slab are reported in Table 1.

Table 1: properties of the Silicon photoconductor slab employed in the PCDM

Property	value
Diameter (mm)	25.4
Thickness (mm)	3
Capacitance (pF)	13
Structure	Single Crystal
Resistivity (Ohm cm)	$>10^4$

On one side of the Silicon slab, a conductive ITO coating has been deposited by sputtering followed by an annealing at 400°C for one hour. The thickness of the ITO layer is in the 100 nm range and the final resistance is 100 Ω /sq. The transmittance of the bare and coated silicon substrates is reported in Figure 2.

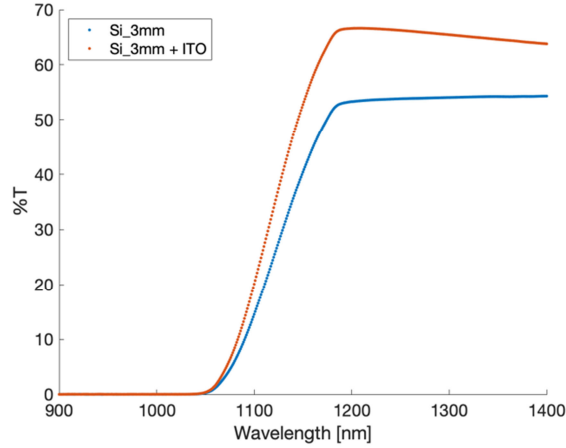


Figure 2: transmission spectra of the silicon photoconductor uncoated (blue curve) and coated (orange curve).

As expected, the transmittance increases when the ITO coating is applied thanks to the reduction of the reflection losses.

2.2 Reflective membrane

The membrane used in our PCDM were purchased from National Photocolor. They are a 5 μm thick nitrocellulose layer with a reflective Al coating. The membrane is mounted on a rigid aluminium ring with a 25.4 mm internal diameter and 35 mm outside diameter.

The membranes were characterized in terms of wavefront without voltage applied and tension. These tasks were carried out using an aluminium dummy photoconductor (uniform load) and a Zygo GPI interferometer. The wavefront of the bare membrane is reported in Figure 3.

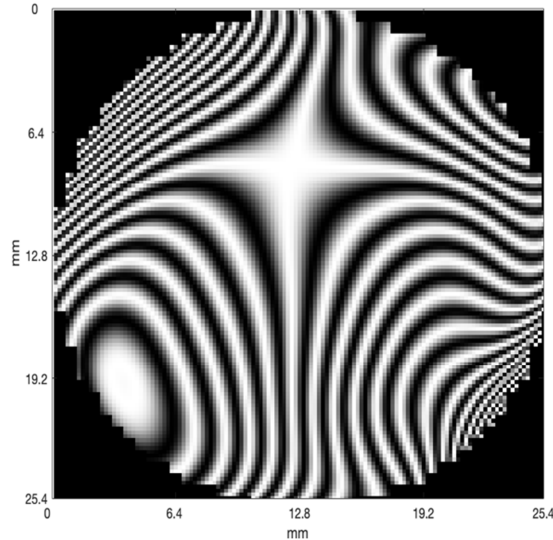


Figure 3: the interference fringe map of the membrane, see the interference fringes for the mounted membrane without any applied electric field, without voltage being applied and in dark conditions.

The wavefront is astigmatic probably due to the gluing of the membrane to the supporting ring. The astigmatism of the membrane introduces a Peak-to-Valley (PV) deformation of 940 nm. To evaluate the membrane tension, a DC voltage between 0 to 180V were applied in ten steps to a dummy aluminium disk electrically coupled with the membrane. Its maximum displacement was measured at the centre as a function of the applied electric field and the data fit with the thin membrane equation:

$$T = \frac{\varepsilon \phi^2 V^2}{32 d^2 M} \quad (1)$$

where ε is the dielectric constant, ϕ the membrane diameter, V the supply voltage, d the distance between the dummy photoconductor and the membrane and M the maximum static deformation. From the tension values, the first resonance frequency in vacuum was also calculated make use of the formula:

$$f_0 = \frac{2.4}{\pi \phi} \sqrt{\frac{T}{\sigma}} \quad (2)$$

where σ is the mass/surface ratio (for nitrocellulose σ is 1230 Kg/m^2). The results for the employed membrane are summarized in Table 2.

Table 2: properties of the membrane employed in the PCDM

Property	Value
Diameter (mm)	25.4
Tension [N/m]	77
Resonance frequency [Hz]*	3370
σ [Kg/m^2]	1230
* It is calculated considering the membrane in vacuum	

2.3 Mechanical design, Interfaces and assembling

The design of the PCDM device needs to guarantee some mechanical specifications, in particular:

- Guarantee the stability in position of the components during the installation procedure;
- Keep the charged surfaces (photoconductor and reflective membrane) well isolated between each other;
- Guarantee the possibility to align and compensate the manufacturing tolerance for both the photoconductor and the membrane;
- Keep the mechanics centered and able to be aligned with respect to the external optical device.

For this reason, the adopted strategy was to use calibrated shims between the photoconductor and the membrane supports. These calibrated shims are able to guarantee a tip/tilt resolution of 0.1 mrad . A key part of the PCDM device was the holder for the membrane and the photoconductor that must be made of a non-conductive material. We opted for acrylonitrile butadiene styrene (ABS). The mounting allows for shining the photoconductor from the back. More details on the mechanical aspects are reported in a previous publication [23]. Figure 4 shows the 3D printed components of the PCDM and the exploded view drawing of the assembled PCDM.

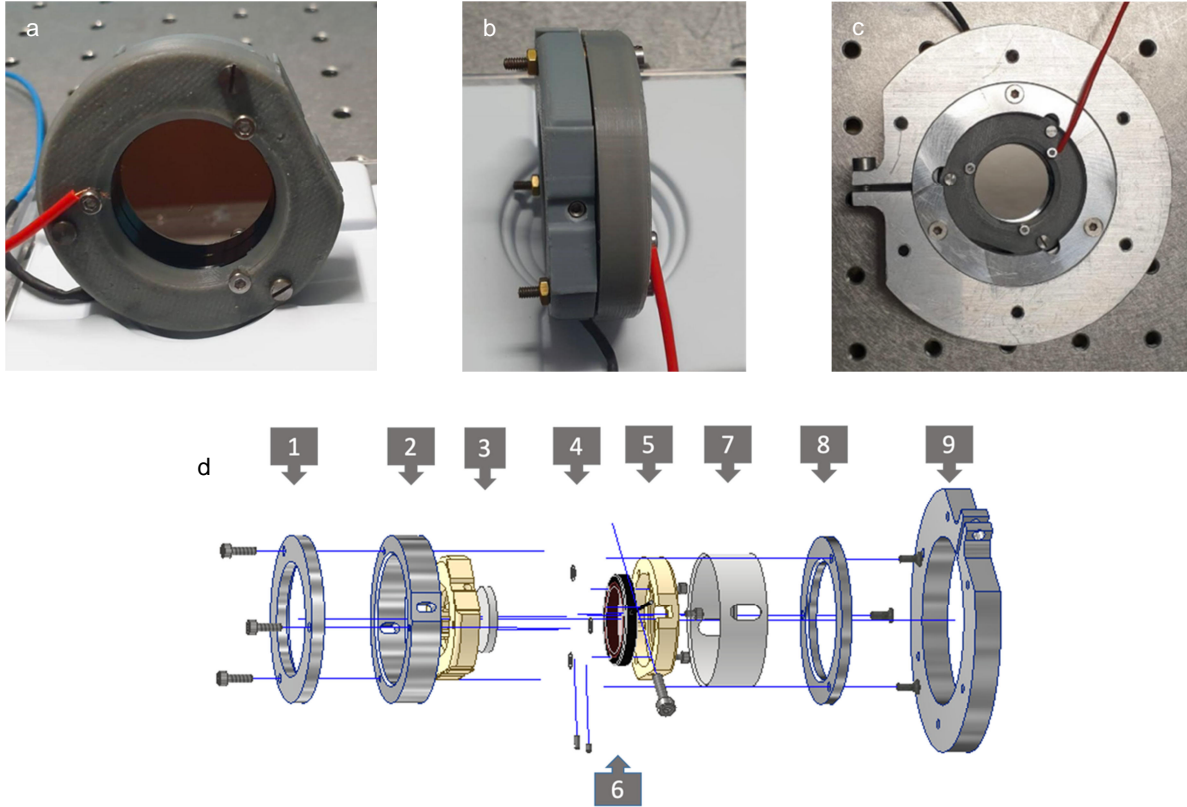


Figure 4: images of the back side (a) and lateral side (b) of the 3D printed components, image of the assembled PCDM in its optomechanics (c), and exploded view drawing of the assembled PCDM design (d), where the listed components are: 1. Screw with membrane side Al ring, 2. Main Al cylinder support, 3. Photoconductor and ABS Photoconductor support, 4 Separating shims, 5. Membrane ABS holder, 6. Membrane, 7. Plastic cover body, 8. Screw with photoconductor side Al ring, and 9. Mechanical adapter holder.

2.4 Characterization setup

The characterization of the PCDM were performed measuring the wavefront of a collimated He-Ne laser beam reflected by the membrane. The wavefront was recorded by means of the PhotonLoop Shack-Hartman wavefront sensor [SHWS]. It is equipped with an iDS UI-3060 CMOS camera controlled by the PhotonProbe software [24]. The main features of the Shack-Hartman device are reported in Table 3.

Table 3: Main features of the Shack-Hartman wavefront sensor.

Property	value
Pixel sensor	1535x1216
Pixel size (μm)	5.86
Lenslet pitch (μm)	150
Focal length (mm)	5.2
Optical area (mm \times mm)	9x7.1
Max number of centroids	48x60
Max framerate	100Hz with 1200 centroids

The scheme of the optical set up is reported in Figure 5 and described in [25].

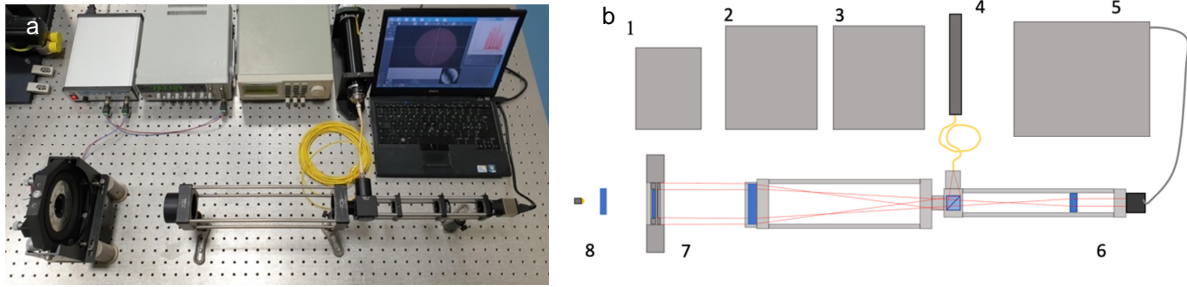


Figure 5 Photo a) and scheme b) of the measurement setup with the main components: 1) amplifier, 2) function generator, 3) DC power supply, 4) laser, 5) PC, 6) Shack-Hartmann, 7) PCDM and PCDM support, and 8) Light source and collimation lens.

The PCDM was fed with an AC voltage obtained by the combination of a function generator (Votcraft FG8210) and a voltage amplifier (Falco Systems WMA-100). For the characterization measurements the range of the applied voltage was from -180 up to 180 V and the frequency from 3 kHz to 30 kHz.

The illumination of the devices was performed on the back side (surface with the conductive ITO coating) of the silicon photoconductor with a NIR LED or lasers. The LED (Roithner LaserTechnik smb1n-940d-02) emits light peaked at 940 nm and provides an irradiance in the range of $2.8 - 8.45 \text{ mW/cm}^2$ on the ITO coating. The two lasers have a wavelength of 532 nm and 1064 nm, the first with a power of 110mW and the latter of 11mW. The spot diameter is 2.5 mm. The switching on and off of the LED and the duty cycle was achieved by means of a microcontroller board (Arduino Mega 2560).

The time response of the PCDM was evaluated using a fast photodiode as a detector. The photodiode is a Texas Instruments OPT101P, with a bandwidth of 14 kHz and a rise and fall time (10%-90%) of 28 μs . To perform this measurement, the 940 nm LED was used to illuminate the PCDM. The LED showed a response time $< 100 \mu\text{s}$.

When the light is illuminating the photoconductor of the PCDM, the curvature of the membrane changes; in order to discriminate between the ON and OFF states of the device, we locate a filtering hole in an intermediate focal plane. By turning on the illumination a drop of the analog output of the signal generated by the photodiode was detected. The temporal response of the PCDM could then be recorded.

3. Results and discussion

The PCDM was firstly characterized in terms of maximum deformation as function of the driving parameters. The photoconductor was illuminated on the back side with a uniform light at 940 nm as described in the previous section.

Figure 6 shows the interference fringes for the membrane measured with the SHWS under various conditions of applied voltage and illumination. Figure 6a shows the interference fringes when a voltage of 120 V at 20 kHz is applied, in dark conditions and without absolute reference, Figure 6b shows the interference fringes in the same conditions but with a light intensity of 5.63 mW/cm^2 , Figure 6c shows the difference between cases b) and a).

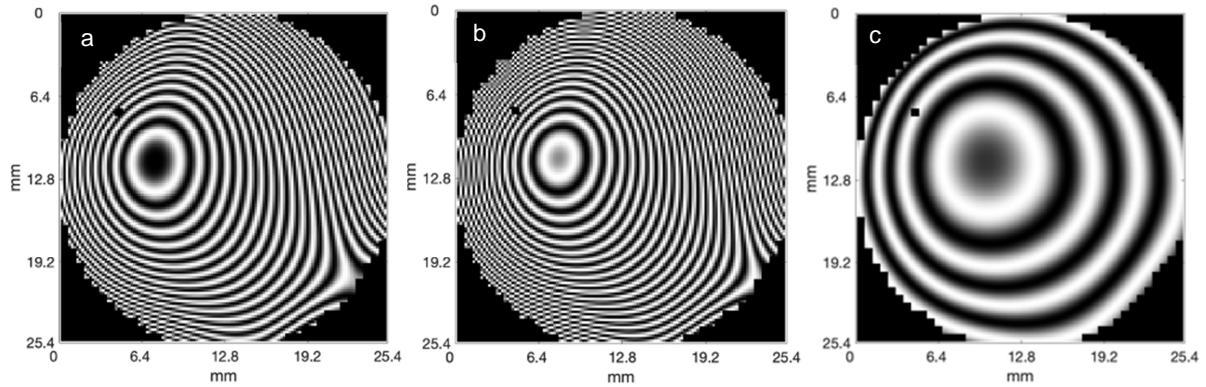


Figure 6: interference fringes of the membrane #2 with an applied voltage of 120 V at 20KHz: in dark condition without absolute reference(a), with a light intensity of 5.63 mW/cm² without absolute reference (b), with a light intensity of 5.63 mW/cm² after had acquired as absolute reference the condition a (c).

In order to characterize the PCDM, the SHWS was set to zero in dark condition with the AC voltage applied; therefore, once the light was turned on, the measured deformation was only due to the illumination. The run consisted in collecting the wavefront sampled at 10 Hz in 20 on-off cycles (1 second with the light on and 1 second with light off). After we have acquired the wavefront, the mirror surface is reconstructed using the first 37 orders of the Zernike polynomials calculated and recorded by the PhotonProbe software of our SHWS. Then, we were able to retrieve the maximum deformation of the membrane, i.e., the difference in Z from the edge to the center of the membrane, with respect to time (see Figure 7a). Finally, for each on-off cycle was computed the mean value and the standard deviation of the maximum membrane deformation of each on-off cycle.

In the bottom of Figure 7, the trends of this parameter with the applied voltage, its frequency and light irradiance are reported.

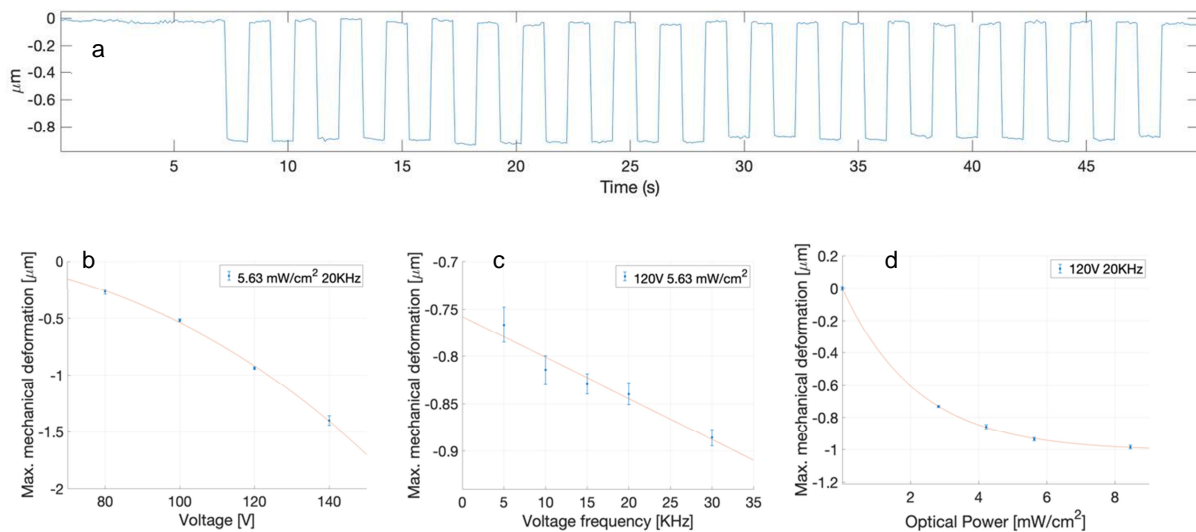


Figure 7: An example of the measurements performed to retrieve the plots with 20 cycles 1s ON + 1s OFF (a). Root mean square (rms) of the maximum deformation of the membrane and their fit (red lines) as function of the applied voltage (AC, peak) (b), voltage frequency (sinusoidal) (c), and irradiance at 940 nm (d). The bars represent the standard deviations of the rms with respect to each set of 20 on-off cycles. The mechanical deformation, in the parameter's interval considered, shows a square dependence with the applied voltage, a linear dependence with the voltage frequency and a negative exponential dependence with the Optical Power.

We notice an increase of the deformation with the applied voltage and this is consistent with the working mechanism of the PCDM and in agreement with the results reported on similar devices [21]. The deformation also increases with the AC frequency and this can be explained considering that the resistance of the silicon is not very high, but it becomes less and less important when increasing the frequency with respect to the capacitor impedance. It

is important to stress the fact that the frequencies are well above the resonance frequency of the membranes. We have an increase of the deformation with the LED irradiance and the trend is towards a plateau, probably due to the saturation effect of the photovoltage responsivity, and photocurrent responsivity [26]. Again, this is consistent with the charge generation and transport and it has been found in other PCDMs [21][22].

Concerning the values, we obtain a maximum mechanical deformation in the center of the membrane up to $1.4 \mu\text{m}$, this value is below the deformation obtained in similar membrane DMs, such as OKO which reach deformations of the order of $10 \mu\text{m}$ [10], but comparable with the surface micro-machined continuous-membrane DMs, such as Boston Micromachines. We have to consider that, in PCDM, the applied voltage induces a constant deformation, which is not present in the common electrostatic membrane mirrors.

Another important task was the determination of the temporal stability of the induced deformation. This was evaluated performing a sequence of 30 seconds light ON and 30 second light OFF and calculating the stability of the maximum deformation. In Figure 8, we report the results for two datasets.

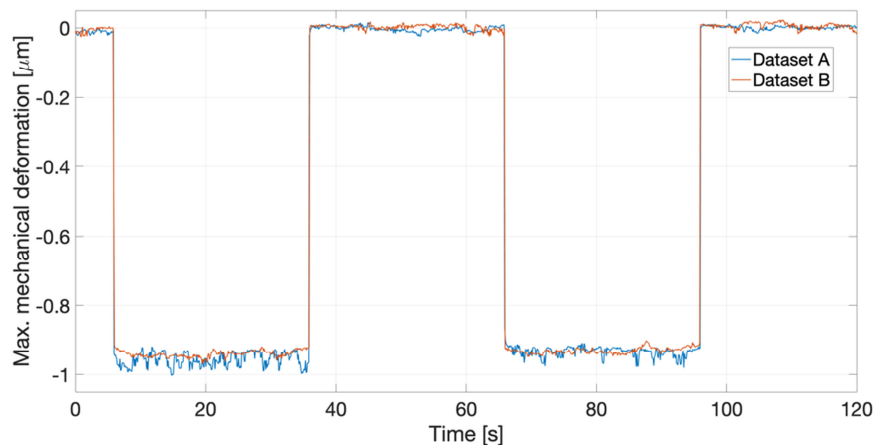


Figure 8: maximum deformation as function of time with 30 seconds ON-OFF cycles for the two datasets (the blue line shows the dataset A, while the orange the dataset B). The PCDM is driven at 120 V, 20 kHz and light intensity of 5.63 mW/cm^2 .

The results are comparable in terms of achieved deformation. Concerning the stability, the dataset A shows a rms value of $0.022 \mu\text{m}$ and a PV of $0.084 \mu\text{m}$ in the ON state and a rms value of $0.012 \mu\text{m}$ and a PV of $0.039 \mu\text{m}$ in the OFF state, while for the dataset B shows a rms value of $0.010 \mu\text{m}$ and an PV of $0.050 \mu\text{m}$ in the ON state and a rms value of $0.007 \mu\text{m}$ and a PV of $0.041 \mu\text{m}$ in the OFF state. The first dataset is noisier in the ON state than the second, which shows similar values for the ON and OFF states. This is linked to a relative instability of the the location of the maximum deformation, probably due to the environmental factors (e.g., vibrations, air turbulence and light intensity variation). This time scale is sufficient for applications in adaptive optics where the refresh rate is of the order of 0.1 – 1 kHz.

For testing the long-term stability of the device, a set of 220 1s on – 1s off repetitions was performed. The results are reported in Figure 9 in terms of maximum deformation.

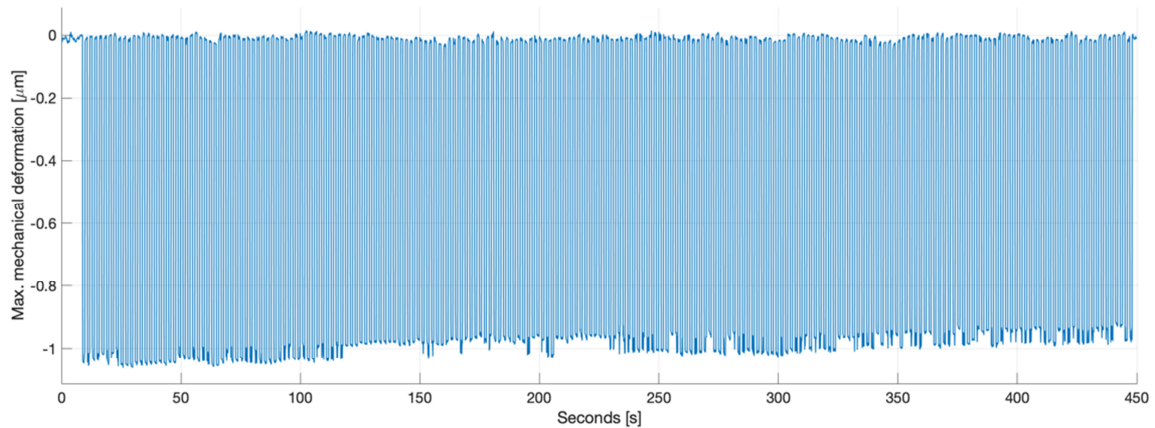


Figure 9: maximum deformation for a set of 220 repetition on-off (2 seconds total period). The PCDM is driven at 120 V, 20 kHz. Light intensity of 5.63 mW/cm^2 .

We see the very high stability of the undeformed position (light OFF) consistent with the previous results and a noisier value for the ON state with a slight drift towards smaller deformations (the maximum mechanical deformation was decreased less than 8%). Indeed, the average value for the OFF and ON states are $0.0488 \pm 0.0212 \mu\text{m}$ and $1.0297 \pm 0.0379 \mu\text{m}$ respectively. This outcome is not so critical in the case of closed loop adaptive optics system, where the deformation is driven at a high rate.

After the tests with the uniform illumination that showed the general performances of the PCDM, lasers at 532 nm (110mW) and 1064 nm (11mW) were projected on the back side of the device in order to probe the deformation with a confined virtual actuator. The spot size was 2.5 mm in diameter and it was scanned along the wafer radius. The membrane deformation was evaluated following the established protocol. In Figure 10, the deformation profile is reported for the different spot positions.

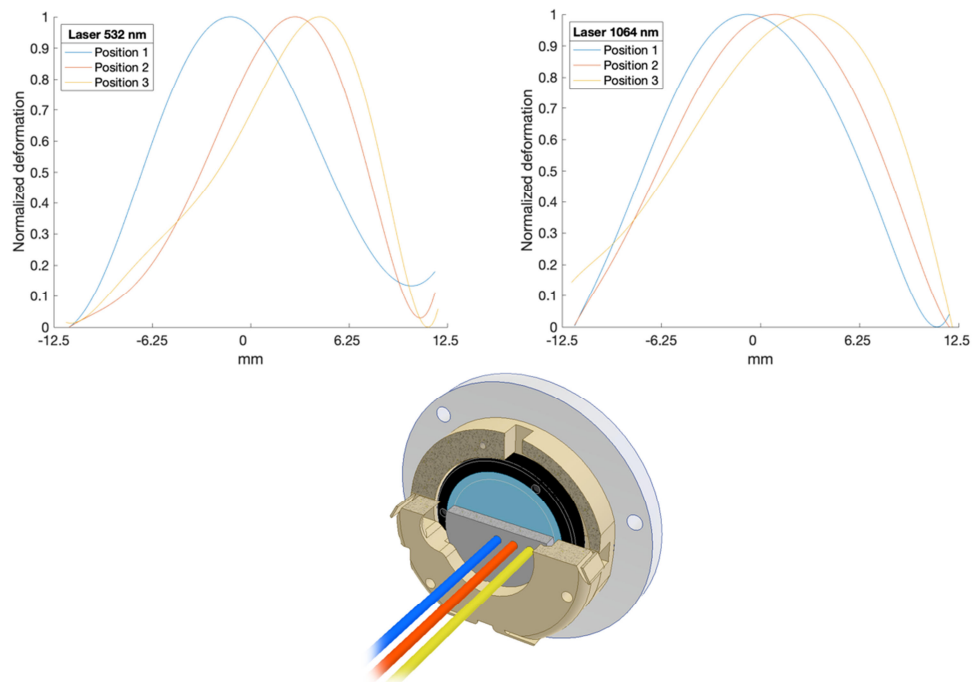


Figure 10: on top: plot profiles of the deformed membrane for three different illuminations with laser spots (532 nm, 1064 nm). On the bottom: Scheme of the PCDM reporting the position where the laser spots illuminated the photoconductor (the blue beam shows the position 1, while the one orange the position 2 and the yellow the position 3).

We notice how the deformation is well localized in the illuminated area, but it is spread over almost half of the membrane area, illustrating a very large influence function. Considering the Full Width at Half Maximum (FWHM), it is about 12 mm, which is half of the PCDM diameter. This could be due to the spread of the charges in the horizontal direction after the photogeneration along the photoconductor substrate, due to the relative high mobility in this direction promoting the charge diffusion and the fact that the sinusoidal vertical electric field is not very high. Indeed, at 20 kHz the voltage drop across the photoconductor is about 12% of the applied voltage, meaning that for an AC 120 V, only 10 V drops on the photoconductor. We can then locate about 10 lasers spots on the surface, i.e., ten actuators, with a potential correction of focus and other low orders aberrations. Some strategies could be possible to improve the confinement and to narrow the influence functions with respect to the illumination pattern dimensions.

The employed lasers at 532 nm and 1064 nm to generate a confined virtual actuator have a higher power than the extended LEDs, but as shown in Figure 7d, we reached the plateau value of the deformation according to the exponential trend with these powers. Therefore, we can induce a similar deformation with much smaller intensities of the order of some mW/cm^2 .

The last test concerned the time response of the device and it has been evaluated following the procedure reported in the Materials and Methods section. In Figure 11, the signal of the photodiode as a function of time is reported.

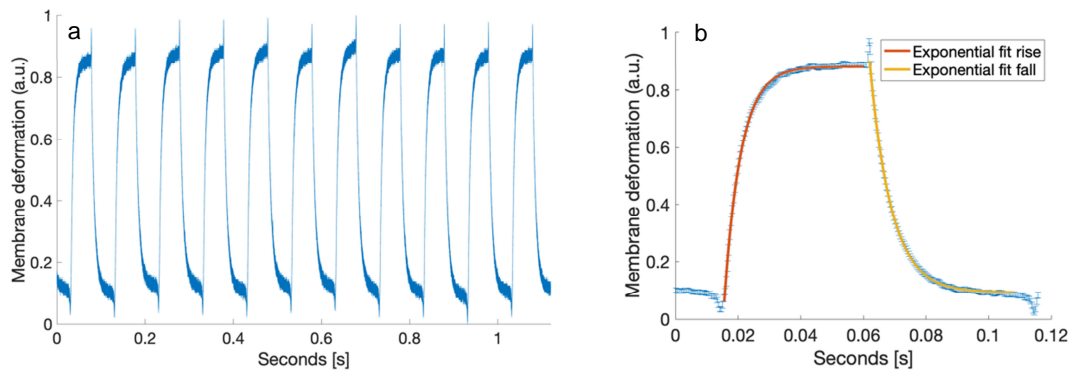


Figure 11: photodiode signal with the DMD always on and the led switch on-off by the Arduino bord (a), fits of the membrane maximum mechanical deformation during the lighting on (red) and lighting off (yellow), The PCDM is driven at 120 V, 10 Hz. Light intensity of $5.63 \text{ mW}/\text{cm}^2$ at 940 nm.

The intensity drop-rise measured by the photodiode is sudden after the light OFF-ON trigger on the PCDM. The temporal response was characterized by illuminating the PCDM locally on an area of 1 cm^2 , simulating the action of a single conventional actuator and measuring the membrane shape variation when the light stimulus is applied (rise time) and when light is removed (fall time).

The time response of the device was quantified fitting each single cycle with a simple negative exponential function both for the rise and fall and then averaging the time constant τ parameter. The average τ is equal to $0.0052 \pm 0.0003 \text{ s}$ for the fall and 0.0065 ± 0.0006 for the rise. Considering the 10% to 90% deformation (it is equal to 2.2τ), we obtain $0.0115 \pm 0.0005 \text{ s}$ and $0.0142 \pm 0.0012 \text{ s}$ respectively. We notice a slighter slower process when the light is turned OFF and this is consistent with other results reported in the literature [21] and can be ascribed to the force that is opposite to the applied pressure. We can conclude that the average frequency for the full deformation range is of the order of 100 Hz.

Conclusions

We have proposed and fabricated a photo-controlled deformable mirror (PCDM) based on an intrinsic 1-inch silicon wafer. A dedicated optomechanical design was performed in order to control the key parameters that affect the PCDM response. The device worked in the AC regime and the deformation was induced by illuminating it with both a NIR LED (940 nm) and lasers (532 nm, 1064 nm). The maximum deformation induced by a uniform illumination was measured by a SHWF and it was a function of the driving voltage, its frequency and the light irradiance, which was the most effective parameter. The largest value was about 2 μm , which is comparable with other deformable mirrors and it allows for a fine control of the mirror focus. By the laser measurements, we identified a low confinement of the deformation, which turned into large influence function that makes the device suitable only for low orders correction of the wavefront. The response time of the Si based PCDM was of the order of 10 ms for the 10%-90% deformation, which turns into a working frequency of 100 Hz.

Acknowledgements

We are grateful to Dario Natali for the fruitful discussion on the electric behaviour of the device. This work was partially supported by OPTICON project (funded by the European Union's Horizon 2020 research and innovation programme under grant agreement No 730890)

References

- [1] Tyson R. Adaptive optics engineering handbook. vol. 67. CRC Press; 1999.
- [2] Dalimier E, Dainty C. Comparative analysis of deformable mirrors for ocular adaptive optics. *Optics Express* 2005;13:4275–85.
- [3] Brida D, Cirimi G, Manzoni C, Bonora S, Villaresi P, De Silvestri S, et al. Sub-two-cycle light pulses at 1.6 μm from an optical parametric amplifier. *Optics Letters* 2008;33:741–3.
- [4] Rigaut F, Neichel B. Multiconjugate adaptive optics for astronomy. *Annual Review of Astronomy and Astrophysics* 2018;56:277–314.
- [5] Madec P-Y. Overview of deformable mirror technologies for adaptive optics and astronomy. *Adaptive Optics Systems III*, vol. 8447, 2012, p. 844705.
- [6] Biasi R, Gallieni D, Salinari P, Riccardi A, Mantegazza P. Contactless thin adaptive mirror technology: past, present, and future. *Adaptive Optics Systems II*, vol. 7736, 2010, p. 77362B.
- [7] Wlodarczyk KL, Bryce E, Schwartz N, Strachan M, Hutson D, Maier RRJ, et al. Scalable stacked array piezoelectric deformable mirror for astronomy and laser processing applications. *Review of Scientific Instruments* 2014;85:24502.
- [8] Zhu Z, Li Y, Chen J, Ma J, Chu J. Development of a unimorph deformable mirror with water cooling. *Optics Express* 2017;25:29916–26.
- [9] Motamedi ME. MOEMS: Micro-opto-electro-mechanical Systems. vol. 126. SPIE press; 2005.
- [10] Vdovin G, Loktev M. Deformable mirror with thermal actuators. *Optics Letters* 2002;27:677–9.
- [11] Helmbrecht MA, He M, Kempf CJ, Marchis F. Long-term stability and temperature variability of Iris AO segmented MEMS deformable mirrors. *Adaptive Optics Systems V*, vol. 9909, 2016, p. 990981.

- [12] Cornelissen SA, Bifano TG, Bierden PA. MEMS deformable mirror actuators with enhanced reliability. *MEMS Adaptive Optics VI*, vol. 8253, 2012, p. 825306.
- [13] Macintosh B, Graham J, Palmer D, Doyon R, Gavel D, Larkin J, et al. The Gemini planet imager. *Advances in Adaptive Optics II*, vol. 6272, 2006, p. 62720L.
- [14] Vidal F, Raffard J, Gendron E, Thijs S, Lapeyrère V, Buey J-T, et al. Tests and characterisations of the ALPAO 64 x 64 deformable mirror, the MICADO-MAORY SCAO AIT facility. *Proceedings of the AO4ELT6 conference*, 2019, p. E4.
- [15] Bortolozzo U, Bonora S, Huignard JP, Residori S. Continuous photocontrolled deformable membrane mirror. *Applied Physics Letters* 2010;96:251108.
- [16] Chanteloup J-C, Baldis H, Migus A, Mourou G, Loiseaux B, Huignard J-P. Nearly diffraction-limited laser focal spot obtained by use of an optically addressed light valve in an adaptive-optics loop. *Optics Letters* 1998;23:475–7.
- [17] Bonora S, Coburn D, Bortolozzo U, Dainty C, Residori S. High resolution wavefront correction with photocontrolled deformable mirror. *Optics Express* 2012;20:5178–88.
- [18] Hardy JW. *Adaptive optics for astronomical telescopes*. vol. 16. Oxford University Press on Demand; 1998.
- [19] Quintavalla M, Bonora S, Natali D, Bianco A. Photo controlled deformable mirrors: materials choice and device modeling. *Optical Materials Express* 2016;6:620–8.
- [20] Haji-Saeed B, Kolluru R, Pyburn D, Leon R, Sengupta SK, Testorf ME, et al. Photoconductive optically driven deformable membrane for spatial light modulator applications utilizing GaAs and InP substrates. *Optical Pattern Recognition XV*, vol. 5437, 2004, p. 115–22.
- [21] Quintavalla M, Bonora S, Natali D, Bianco A. Zinc selenide-based large aperture photo-controlled deformable mirror. *Optics Letters* 2016;41:2573.
- [22] Quintavalla M, Baratto M, Natali D, Bonora S, Bertarelli C, Bianco A. Fully Organic Photocontrolled Deformable Mirror. *Advanced Optical Materials* 2018;6:1800361.
- [23] Redaelli E, Cabona L, Olivieri M, Pariani G, Natali D, Zamkotsian F, et al. Photo-controlled deformable mirror based on silicon photoconductor. *Adaptive Optics Systems VII*, vol. 11448, 2020, p. 114485S.
- [24] Mocci J, Quintavalla M, Trestino C, Bonora S, Muradore R. A multiplatform CPU-based architecture for cost-effective adaptive optics systems. *IEEE Transactions on Industrial Informatics* 2018;14:4431–9.
- [25] Zamkotsian F, Cabona L, Redaelli E, Pariani G, Lanzoni P, Bianco A. Photo-controlled deformable mirror for wavefront shaping. *MOEMS and Miniaturized Systems XX*, vol. 11697, 2021, p. 1169703.
- [26] Paschotta R. *Encyclopedia of Laser Physics and Technology - responsivity, photodetectors, photodiodes, sensitivity* 2018. www.rp-photonics.com.